Original papers
Materials for energy and environment, next-generation photovoltaics, and green technologies

УДК 546.05 DOI: 10.17277/jamt.2023.04.pp.279-293

A method of obtaining aluminum tris(8-hydroxyquinoline) and its physicochemical properties

© Denis V. Belov[ab]✉, Sergey N. Belyaev[ab], Pavel A. Yunin[b], Dmitriy B. Radishev[a]

[a] *Federal Research Center A.V. Gaponov-Grekhov Institute of Applied Physics of the Russian Academy of Sciences, 46, Ulyanova St., Nizhny Novgorod, 603950, Russian Federation,*
[b] *The Institute for Physics of Microstructures of the Russian Academy of Sciences, Nizhny Novgorod, 603950, Russian Federation*

✉ bdv@ipfran.ru

Abstract: Obtaining high-purity single-crystalline aluminum tris(8-hydroxyquinolinate) (Alq_3) in significant volumes is a topical task both for OLED technologies and for its use as a promising electron-pumped laser material. This article proposes a simple, convenient and ecologically friendly "one-pot" synthesis based on the interaction of high-purity aluminum powder and 8-hydroxyquinoline in an aqueous solvent of ammonia with high yield. The method allows for the selective synthesis of an α-polymorphic modification of the meridional isomer Alq_3. An electron microscopic study of the α-phase powder *mer*-Alq_3 was carried out. It has been determined that the substance has a uniform morphology of a tree-like branching structure formed from rod-like linear crystals. The structure of the resulting compound was characterized by X-ray diffraction, Raman spectroscopy, and electron spectroscopy. Qualitative and semi-quantitative analysis of chemical elements was carried out using energy-dispersive X-ray spectroscopy (EDX method). The optical absorption spectra of Alq_3 solvents in eight organic solvents were studied: DMSO, CH_3CN, EtOH, *i*-PrOH, TEP, $CHCl_3$, 1,4-dioxane, and toluene. The molar extinction coefficients of α-Alq_3 in organic solvents were calculated in the short-wave and visible regions of the spectrum. The solvatochromic effect in the studied systems was assessed. A methodologyfor the quantitative determination of Alq_3 in organic solvents and standardization of its solvents has been developed by the spectrophotometric method.

Keywords: one-pot synthesis; aluminum tris(8-hydroxyquinoline); *mer*-Alq_3; 8-hydroxyquinoline; Raman spectroscopy; UV/VIS; OLED; OLED.

For citation: Belov DV, Belyaev SN, Yunin PA, Radishev DB. Obtaining method and physicochemical properties of aluminum tris(8-hydroxyquinoline). *Journal of Advanced Materials and Technologies*. 2023;8(4):279-293. DOI: 10.17277/jamt.2023.04.pp.279-293

Способ получения и физико-химические свойства трис(8-гидроксихинолината) алюминия

© Д. В. Белов[ab]✉, С. Н. Беляев[ab], П. А. Юнин[b], Д. Б. Радищев[a]

[a] *Институт прикладной физики им. А. В. Гапонова-Грехова РАН, ул. Ульянова, 46, Нижний Новгород, 603950, Российская Федерация,*
[b] *Институт физики микроструктур РАН, ГСП-105, Нижний Новгород, 603950, Российская Федерация*

✉ bdv@ipfran.ru

Аннотация: Получение высокочистого монокристаллического трис(8-гидроксихинолината) алюминия (Alq_3) в значительных объемах является актуальной задачей как для ОСИД-технологий, так и для его применения в качестве перспективного лазерного материала с электронной накачкой. В статье предложен простой, удобный и экологичный «one-pot» синтез, основанный на взаимодействии порошка высокочистого алюминия и 8-гидроксихинолина в водном растворе аммиака с высоким выходом. Метод позволяет осуществлять селективный синтез α-полиморфной модификации меридионального изомера Alq_3. Проведено электронно-микроскопическое

исследование порошка α-фазы *mer*-Alq_3. Определено, что вещество имеет однородную морфологию древовидной ветвящейся структуры, образованной из стержневидных линейных кристаллов. Структура полученного соединения охарактеризована методами рентгеновской дифракции, спектроскопии комбинационного рассеивания света и электронной спектроскопии. Методом энергодисперсионной рентгеновской спектроскопии (EDX-метод) проведен качественный и полуколичественный анализ химических элементов. Изучены спектры оптического поглощения растворов Alq_3 в восьми органических растворителях: ДМСО, CH_3CN, EtOH, *i*-PrOH, ТЭФ, $CHCl_3$, 1,4-диоксан, толуол. Рассчитаны коэффициенты молярной экстинкции α-Alq_3 в органических растворителях в коротковолновой и видимой областях спектра. Проведена оценка сольватохромного эффекта в изученных системах. Разработана методика количественного определения Alq_3 в органических растворителях и стандартизации его растворов спектрофотометрическим методом.

Ключевые слова: «one-pot» синтез; трис(8-гидроксихинолинат) алюминия; *mer*-Alq_3; 8-гидроксихинолин; КР-спектроскопия; UV/VIS; ОСИД; OLED.

Для цитирования: Belov DV, Belyaev SN, Yunin PA, Radishev DB. Obtaining method and physicochemical properties of aluminum tris(8-hydroxyquinoline). *Journal of Advanced Materials and Technologies*. 2023;8(4):279-293. DOI: 10.17277/jamt.2023.04.pp.279-293

1. Introduction

The studies of Tang and Van Slyke in 1987 [1], who discovered the intense electroluminescence of aluminum tris(8-hydroxyquinolinate), began the era of developing new light-emitting devices – Organic Light Emitting Diodes (OLEDs). Recently, technical products based on the use of organic electroluminophores have become of great practical importance. Based on them, new highly efficient light sources and information display devices are being developed.

Compared to fluorescent lamps and inorganic light-emitting diodes (LED), OLED devices have a number of advantages: smaller dimensions, weight and power consumption with comparable brightness, better color rendering, low power dissipation of the luminous surface and the ability to create large luminous surfaces (flat displays).

Aluminum tris(8-hydroxyquinolinate) (Alq_3) is one of the most widely used compounds in OLED technology. Due to its thermal stability, ease of synthesis and purification, and exceptional electron transport and electroluminescent properties in thin films, Alq_3 is used as a green organic electroluminescent phosphor and an electron transport layer in the manufacture of OLED devices.

Alq_3 is an organometallic coordination compound that emits green light with a photoluminescence wavelength of about 500 nm. In metal hydroxyquinolinates, hydroxyquinolines act as bidentate ligands and attach to the aluminum atom through oxygen and nitrogen atoms with a coordination number of six. The luminescence ability of $Alq_3$is responsible for the $\pi \rightarrow \pi^*$ electronic transition from the HOMO of the ligand, localized on the phenoxyl ring, to the LUMO, located on the pyridine ring.

Today, the existence of two isomers is known: meridional *mer*-Alq_3 and frontal *fac*-Alq_3 which crystallize in five polymorphic modifications of Alq_3 – α, β, γ, δ, ε [2–5]. Each such phase is stable under certain thermodynamic conditions and has its own spectral characteristics [6].

It is currently known that three of the five polymorphic modifications of crystalline Alq_3 (α, β, ε) are composed of *mer*- isomers (*meridional*) with C1 symmetry [3], and two polymorphic modifications (γ, δ) are composed of *fac*- isomers (*facial*) with C3 symmetry [6]. The phase and impurity purity of Alq_3 determines both the basic functional properties of the compound (luminescence, electron-hole conductivity, etc.) and the durability of the product as a whole.

Various methods for the synthesis of Alq_3 are presented in the literature [7–9], but there is no easy-to-implement method of directed synthesis with controlled phase composition. The task of obtaining high-purity Alq_3 in significant volumes is relevant not only for OLED technologies, but also for further studies of single-crystal Alq_3, which is used as a promising electron-pumped laser material.

The purpose of this work is to obtain Alq_3 in a new, convenient way and to study its structural and optical properties using Raman spectroscopy and UV-visible spectrophotometry.

2. Materials and Methods

2.1. Alq_3 *synthesis*

Sample I. To synthesize the product, the well-known technique proposed in [10] was used. The product was obtained from 8-hydroxyquinoline (HQ) and aluminum salt in an aqueous medium. For this purpose, 1 g of aluminum nitrate $Al(NO_3)_3 \cdot 9H_2O$

was dissolved in 100 mL of deionized H_2O. The solvent was heated to 60 °C. 1.5 g of HQ was dissolved in a mixture consisting of 20 mL of H_2O and 4 mL of glacial acetic acid. The HQ solvent was slowly added drop wise to the aluminum nitrate solvent. The pH of the resulting solvent was then increased to 8 by adding ammonia solvent to precipitate the product Alq_3. The resulting precipitate was thoroughly washed with hot water (60 °C). The bright yellow powder with a melting point > 300 °C was dried in a vacuum oven at a temperature of 130 °C. The yield of Alq_3 was no more than 95 %.

Sample II. 1 g of Al_2O_3 was added to 100 mL of 1 M HCl solvent and heated to 50–60 °C. The solvent was filtered while hot. A 10 % excess of the reagent was added to the resulting filtrate, then a freshly prepared 2 M solvent of CH_3COONH_4 was slowly introduced until a non-disappearing yellow precipitate appeared and an additional 25 mL was added for complete precipitation. The precipitate was filtered, washed with hot water and dried at 120 °C. The reagent was prepared as follows: 12.5 g of HQ was added with stirring to 25 mL of glacial acetic acid with low heating until dissolved. The resulting solvent was poured into 450 ml of deionized H_2O heated to 60 °C. The solvent was cooled, filtered and diluted to 500 mL.

Sample III. Alq_3 synthesis was carried out according to the method [5] in isopropyl alcohol (*i*-PrOH).

Sample IV. Metallic aluminum powder ("PA-HF", 99.99 wt. %) and a 25 % aqueous solvent of ammonia hydrate $NH_3 \cdot H_2O$ ("special purity grade", 99.9 wt. %) were used as starting materials. Alq_3 synthesis was carried out in one step. Aluminum powder was poured (25 °C) into a $NH_3 \cdot H_2O$ solvent, the mixture was heated until its activation it and stirred until intense gas evolution began. A solvent of HQ in a 10 % aqueous solvent of ammonia hydrate was added to the resulting mixture in a molar ratio of Al : HQ = 1 : 3. The initial reagent HQ (pure grade, 99.9 wt. %) was recrystallized from absolute EtOH and dried in vacuum (T_{melt} = 74.5–75 °C). The reaction vessel was then placed on a heating device and kept at boiling temperature for 60 minutes. The synthesis was carried out with constant stirring at a speed of at least 300 rpm. Over time, the solvent became discolored and a yellow-green precipitate formed. The resulting precipitate was filtered, washed with water and dried at a temperature of 120 °C in an argon atmosphere. The synthesis product was a yellow-green crystalline powder (T_{melt} = 300 °C). Recrystallization was carried out from chloroform.

A comparison was made with commercially available Alq_3 (Sigma-Aldrich) with a purity of at least 99.995 %.

During the studies the following organic solvents were used: EtOH (≥ 99.8 %, special purity), *i*-PrOH (≥ 99.8 %, special purity, 11-5 OP-1, JSC "EKOS-1", Russia), CH_3CN (≥ 99.8 %, analytical grade, JSC "EKOS-1", Russia), dimethyl sulfoxide (DMSO) (≥ 99.8 %, UFS, JSC "EKOS-1", Russia), $CHCl_3$ (≥ 99.8 %, reference, JSC "EKOS-1", Russia), 1,4-dioxane (≥ 99.8 %, analytical grade, JSC "EKOS-1", Russia), toluene (≥ 99.8 %, analytical grade, JSC "EKOS-1", Russia), triethyl phosphate (TEP) (≥ 99.8 %, JSC "EKOS-1", Russia). All solvents were purified, dehydrated, and distilled using standard methods before use.

2.2. Analytic methods

X-ray diffraction analysis of powdered samples was carried out on a Bruker D8 Discover diffractometer (CuKα radiation) in Bragg-Brentano geometry with a LynxEye linear position-sensitive detector. The analyzed powders were placed in identical fused quartz cuvettes, and diffraction patterns were recorded by θ/2θ scanning in the angular range from 3° to 50° along the 2θ angle.

The morphology of the synthesized samples was studied using a VEGA 3 XMH (TESCAN) scanning electron microscope (SEM) with a LaB_6 lanthanum hexaboride cathode. The samples were applied to adhesive conductive tape without prior manipulation or mechanical impact. Qualitative and semi-quantitative analysis of chemical elements was carried out by energy dispersive X-ray spectroscopy (EDX method) using an energy dispersive spectrometer based on a semiconductor silicon drift detector with nitrogen-free cooling manufactured by OXFORD INSTRUMENTS, with an accuracy of the mass fraction of elements of 0.1 %, mounted on a scanning electron microscope column with range of detectable elements from Be(4) to Pu(94).

Micrographs of the synthesized Alq_3 samples were obtained using a ZEISS Axio Imager Vario optical microscope. The following researchmethods in reflected light were used: bright field, dark field, polarization contrast, differential interference contrast (Nomarski DIC), circular differential interference contrast (C-DIC).

Raman spectroscopy (Raman spectra) was performed on a Renishaw InVia Reflex instrument (Renishaw plc, UK) with a Leica DMLM confocal microscope with a resolution of up to 2.5 μm. The laser radiation wavelength was 514.5 nm, the radiation power was 0.1–1.0 mW at the measurement point, and the diameter of the analyzing laser beam was ~1 μm.

Electronic absorption spectra (UV/VIS spectra) of Alq_3 were recorded using a UV-3600i Plus spectrophotometer (Shimadzu, Japan) (with a quartz cuvette absorbing layer thickness of 10 mm in dual-beam mode).

3. Results and Discussion

3.1. Crystal structure of synthesized compounds

Figures 1 and 2 demonstrate X-ray diffraction patterns of the synthesized Alq_3 samples. Figure 1 shows diffraction patterns of the synthesized products: samples I – III. All samples differ from each other in the location of the characteristic peaks. However, none of them corresponds to the spectrum characterizing the pure Alq_3 phase. Unidentified and additional peaks can be seen in the spectra. For example, the diffraction pattern shown in Fig. 1 (curve *2*) contains a number of additional peaks in the 2θ range at 8.5–11°, 17–18°, 21–23°, 24°, 31–35°. The presence of additional peaks, their modification and disappearance indicates the presence of impurities and residual solvents [11].

Figure 2 (curve *2*) shows the diffraction pattern of Alq_3 (sample IV) obtained by the proposed method. For comparison, Fig. 2 also demonstrates a powder diffraction pattern (curve *1*) calculated in the "Diffrac. Topas" software package based on CCDC data # 1241652 for single crystals of the α-phase Alq_3 [12]. When calculating the diffraction pattern from the cif file data in "Diffrac. Topas" and fitting it to the experiment, the fundamental parameters approach was used. At the same time, instrumental parameters were set, i.e. dimensions of the slits (0.6 mm equatorial slit on the primary beam and the axial Soller slit 2.5°), detector parameters (a position-sensitive one-dimensional LynxEYE detector with an aperture of 2° at the angle 2θ was used), taking into account the axial and equatorial divergence of the beam and spectral composition of radiation (CuK_α doublet). When fitting, the parameters of the powder microstructure were varied – the sizes of the regions of coherent scattering and microdeformation (50 nm and 0.2 %, respectively), as well as the approximation of the instrumental background by a 5th order Chebyshev polynomial.

Figure 2 (curve *3*) also shows a diffraction pattern of a commercial sample of the α-polymorphic phase *mer*-Alq_3 (Sigma-Aldrich). One can see an almost complete coincidence of the diffraction pattern of the synthesized α-Alq_3 (sample IV) with the calculation results and the diffraction pattern of the commercial sample.

The crystal structure of the α-phase Alq_3 has triclinic symmetry, space group *P*-1, unit cell parameters: $a = 6.2586(8)$ Å, $b = 12.914(2)$ Å, $c = 14.743(2)$ Å, $\alpha = 109.66(1)°$, $\beta = 89.66(1)°$, $\gamma = 97.68(1)°$ [12].

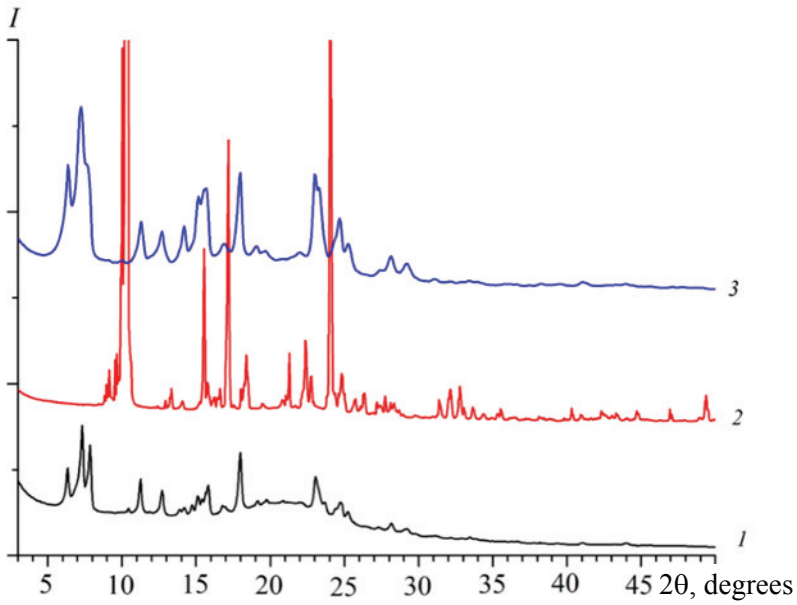

Fig. 1. X-ray diffraction patterns of Alq_3 powder samples: sample I (*1*), sample II (*2*), sample III (*3*)

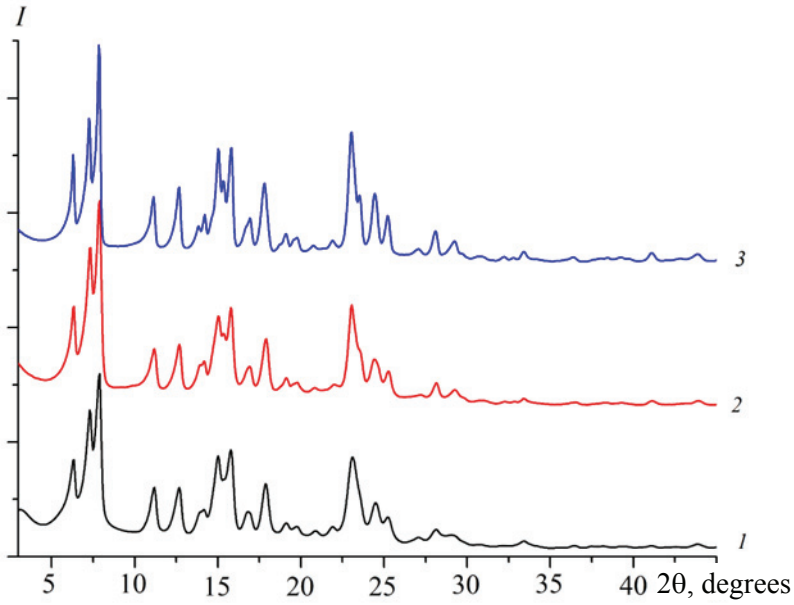

Fig. 2. Powder diffraction patterns of Alq_3: according to the results of calculation in the "Diffrac. Topas" software package based on the data of [12] (*1*), synthesized sample IV (*2*), commercial sample of α-phase Alq_3 "Sigma-Aldrich" (*3*)

According to the powder diffraction data (Fig. 2, curve *2*), the synthesized Alq_3 (sample IV) corresponds to the commercial preparation and calculated data, as indicated by the presence of three intense, well-resolved peaks in the range $6° < 2\theta < 8°$. It is also possible to identify two well-resolved peaks in the range $10° < 2\theta < 13°$, two peaks in the range $13° < 2\theta < 17°$, a characteristic peak at 18° and three well-resolved peaks in the range $23° < 2\theta < 26°$. The data obtained are consistent with previously published works [12–15].

Figure 3 shows the structure and crystal packing of the α-phase of the geometric *mer*-Alq_3 isomer.

Figure 4 shows photographs of *mer*-Alq_3 powder (sample IV). The product crystals have a rod shape with a random distribution. The maximum size of rods is about 100 μm. There are no obvious defects visually observed on the surface of the crystals, which indicates a sufficiently high quality of the resulting *mer*-Alq_3 powder.

Electron microscopic research of the α-phase powder of *mer*-Alq_3 was carried out. Figure 5 shows the corresponding microphotographs. It was determined that the substance has a uniform morphology of a tree-like branching structure formed from rod-like linear crystals. The results of microscopy indicate the absence of impurities that differ in particle shape from the bulk of the substance, and the results of energy-dispersive elemental microanalysis confirm the formation of a powder of the *mer*-Alq_3 α-phase which is homogeneous in chemical composition. In Table 1 shows the data of EDX analysis of the synthesized Alq_3 powder (sample IV).

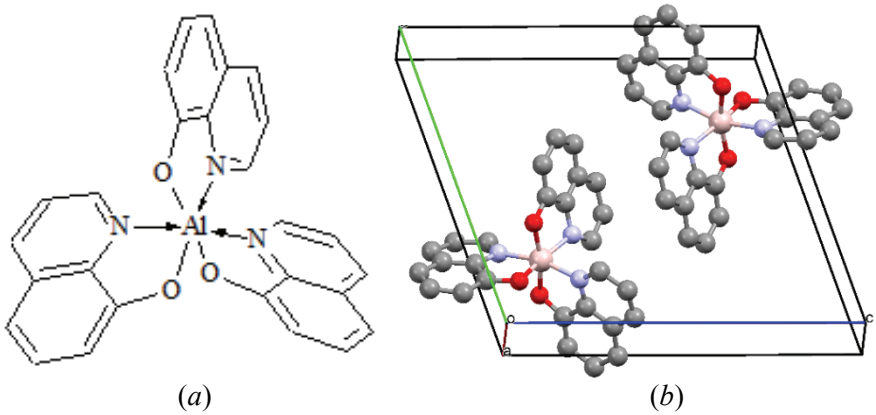

Fig. 3. Chemical structure (*a*) and type of crystal packing of the geometric *mer*-Alq_3 isomer (*b*)

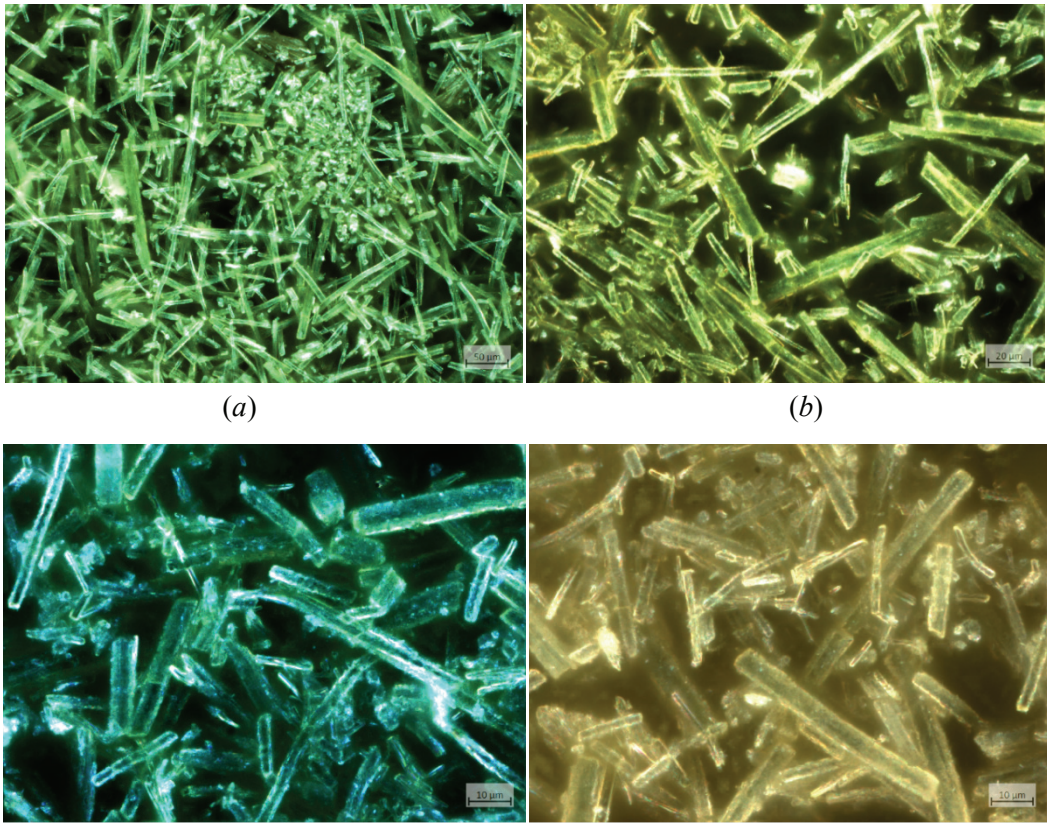

(*a*) (*b*)

(*c*) (*d*)

Fig. 4. Micrographs of *mer*-Alq_3 α-phase powder (sample IV):
×20, 0.5 HD DIC M27 (*a*); ×50, 0.8 HD DIC (*b*); ×100, 0.9 BD DIC (*c*); ×100, 0.9 BD DIC (*d*)

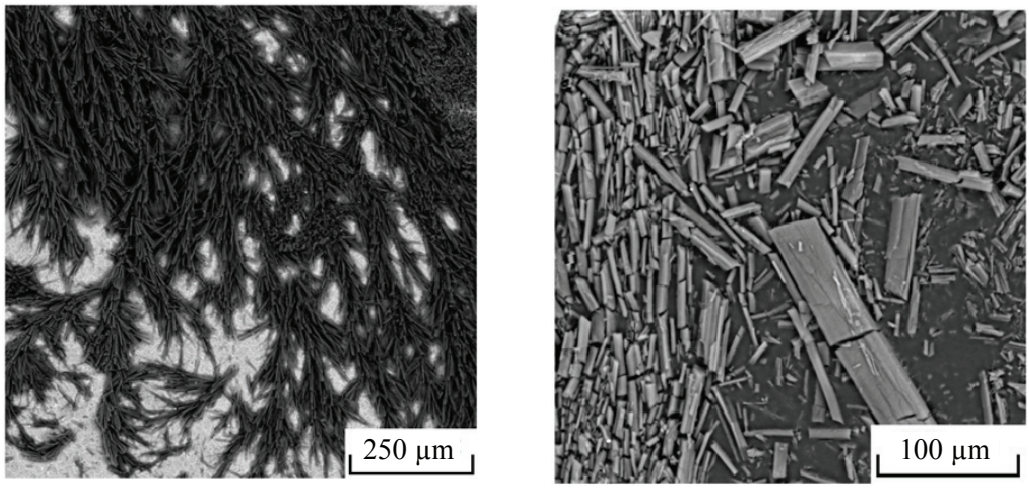

(*a*) (*b*)

Fig. 5. Morphology of *mer*-Alq_3 α-phase powder crystals

Table 1. Results of Alq_3 EDX analysis (molecular formula $C_{27}H_{18}AlN_3O_3$, molecular weight 459.42)

Element	C	Al	N	O
Found (powder), wt. %	70.6 ± 0.01	5.7 ± 0.01	9.2 ± 0.01	10.5 ± 0.01
Calculated, wt. %	70.6	5.7	9.2	10.5

3.2. Raman spectroscopy of HQ and Alq_3

Figure 6 shows the Raman spectra of the synthesized sample of the *mer*-Alq_3 (sample IV) (*1*) α-phase and the original reagent of 8-hydroxyquinoline (HQ) (*2*).

Tables 2 and 3 show the interpretation of the Raman spectra of the synthesized compound, i.e. *mer*-Alq_3 (sample IV) α-phase and 8-hydroxyquinoline (HQ).

Raman spectrum of Alq_3 (Table 2). According to literature data [16], about 150 normal modes can be distinguished in the Raman spectrum of Alq_3, which include vibrations of the hydroxyquinoline fragment and vibrations of the Al–O and Al–N bonds.

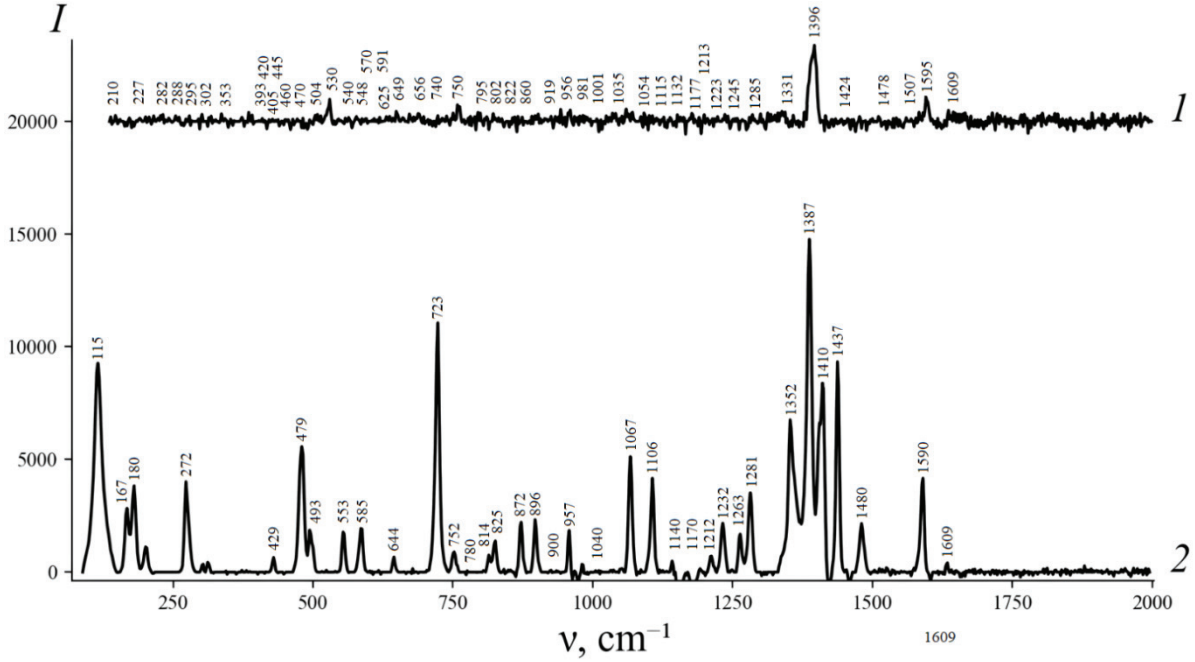

Fig. 6. Raman spectra: α-polymorphic phase of *mer*-Alq_3, sample IV (*1*), 8-hydroxyquinoline (HQ) (*2*)

Table 2. Line frequencies in the Raman spectrum (Fig. 6, spectrum *1*) and Alq_3 vibrational mode assignment (sample IV)

ν, cm^{-1}	Vibrational modes	Line assignment
1609	CC ring stretching, CN ring stretching	ν_{ring}(C–C) + ν(C–N)
1595	Ring stretching, CH wagging	ν_{ring} + δ(C–H)
1507	Ring stretching	ν_{ring}
1478	CH wagging, ring stretching	δ(C–H) + ν_{ring}
1471	CH wagging, ring stretching	δ(C–H) + ν_{ring}
1424	CH wagging, ring stretching	δ(C–H) + ν_{ring}
1396	CH wagging, ring stretching	δ(C–H) + ν_{ring}
1331	Ring stretching, CO stretching, CH wagging	ν_{ring} + ν(C–O) + δ(C–H)
1285	CO stretching, CH wagging	ν(C–O) + δ(C–H)
1245	CN stretching, CH wagging	ν(C–N) + δ(C–H)
1236	CN stretching, CH wagging	ν(C–N) + δ(C–H)
1223	CN stretching, CH wagging	ν(C–N) + δ(C–H)
1213	CN stretching, CH wagging	ν(C–N) + δ(C–H)
1177	CH wagging	δ(C–H)
1132	CH wagging	δ(C–H)
1115	CO stretching, CH wagging	ν(C–O) + δ(C–H)
1054	Ring stretching, CH wagging	ν_{ring} + δ(C–H)
1035	Ring stretching, CH wagging	ν_{ring} + δ(C–H)

Continued Table 2

ν, cm^{-1}	Vibrational modes	Line assignment
1001	CH wagging	$\delta_{wagging}$(C–H)
981	Ring deformation	*RD*
956	CH wagging	$\delta_{wagging}$(C–H)
919	Ring deformation, AlN stretching	*RD* + ν(Al–N)
860	CH wagging	$\delta_{wagging}$(C–H)
822	CH wagging	$\delta_{wagging}$(C–H)
802	Ring deformation	*RD*
795	CH wagging	$\delta_{wagging}$(C–H)
750	Breathing, ring	ν_{ring} (breathing)
740	AlN stretching	ν(Al–N)
656	CH wagging	$\delta_{wagging}$(C–H)
649	AlO stretching, ring deformation	ν(Al–O) + *RD*
625	AlO, AlN stretching, ring deformation	ν(Al–O) + ν(Al–N) + *RD*
591	CH torsion	$(C–H)_{torsion}$
570	Ring deformation, AlOC wagging	*RD* + δ(Al–O–C)
548	AlO, AlN stretching, ring deformation	ν(Al–O) + ν(Al–N) + *RD*
540	AlO, AlN stretching, ring deformation	ν(Al–O) + ν(Al–N) + *RD*
523	Ring deformation, AlO stretching	*RD* + ν(Al–O)
504	Ring deformation	*RD*
470	Ring deformation	*RD*
460	CH torsion	$(C–H)_{torsion}$
445	CH torsion	$(C–H)_{torsion}$
420	AlN stretching, AlOC wagging	ν(Al–N) + δ(Al–O–C)
405	ring deformation, AlO stretching	*RD* + ν(Al–O)
393	ring deformation, AlN stretching	*RD* + ν(Al–N)
353	ring deformation, AlOC wagging	*RD* + δ(Al–O–C)
302	AlN stretching, CCO wagging	ν(Al–N) + δ(C–C–O)
295	Ring torsion	*RT*
288	Ring torsion	*RT*
282	Ring torsion	*RT*
227	Ring wagging	$\delta_{wagging}$(C–C)
210	Ring wagging	$\delta_{wagging}$(C–C)

Table 3. Line frequencies in the Raman spectrum (Fig. 6, spectrum *2*) and correlation of vibrational modes HQ

ν, cm^{-1}	Vibrational modes	Line assignment
1609	CC ring stretching, CH wagging	ν_{ring}(C–C) + δ(C–H)
1590	CC ring stretching, CH wagging	ν_{ring}(C–C)+ δ(C–H)
1480	CC ring stretching	ν_{ring}(C–C)
1437	OH wagging, CC stretching	δ(O–H) + ν_{ring}(C–C)
1410	CC stretching, CC wagging	ν_{ring}(C–C) + δ(C–C)
1387	CC stretching, CC wagging	ν_{ring}(C–C) + δ(C–C)
1352	CC stretching, CO stretching, CH wagging	ν_{ring} + ν_{ring}(C–O) + δ(C–H)
1281	CH wagging, CN stretching	δ(C–H) + ν_{ring}(C–N)
1263	CH wagging	δ(C–H)
1232	CC stretching	ν_{ring}(C–C)
1212	CN, CO stretching	ν_{ring}(C–N) + ν_{ring}(C–O)
1170	CH wagging	δ(C–H)
1140	CH wagging	δ(C–H)

Continued Table 3

ν, cm^{-1}	Vibrational modes	Line assignment
1106	CC stretching, CH wagging	ν_{ring}(C–C) + δ(C–H)
1067	CH wagging	$\delta_{wagging}$(C–H)
1040	CH wagging	$\delta_{wagging}$(C–H)
957	CH wagging	$\delta_{wagging}$(C–H)
900	CH wagging	$\delta_{wagging}$(O–H)
896	CH wagging	$\delta_{wagging}$(C–H)
872	CH wagging	$\delta_{wagging}$(C–H)
825	Ring wagging	$\delta_{bending}$(C–C)
814	Ring deformation	*RD*
780	CH, OH wagging	$\delta_{wagging}$(C–H) + $\delta_{wagging}$(O–H)
752	Breathing, ring wagging	$\delta_{bending}$(C–C)
723	Ring torsion	*RT*
644	Breathing, ring stretching, CH wagging	ν_{ring} + δ(C–H)
585	CO, CH wagging	δ(C–O) + δ(C–H)
553	Ring deformation	*RD*
493	Ring torsion and deformation	*RT* + *RD*
479	CO wagging	$\delta_{wagging}$(C–O)
272	Ring torsion	*RT*
180	Ring torsion	*RT*
167	Ring torsion	*RT*

The modes between 1609 and 1035 cm^{-1} are mainly due to the stretching of C–C bonds of hydroxyquinoline rings and the bending vibrations of C–H bonds (C–H rocking plane vibration, scissor vibration). The characteristic lines in Alq_3 spectrum (Fig. 6, spectrum *1*) at 1595 and 1396 cm^{-1} correspond to the vibrational modes of the aromatic ring [ν_{ring} + δ(C–H)] of 8-hydroxyquinolinate (HQ) ligand, while in the Raman spectrum of HQ (Fig. 6, spectrum *2*) the last peak is shifted to shorter wavelengths and has a maximum at 1387 cm^{-1}. Stretching vibrations of the C–C bond, accompanied by rocking and shear vibrations of the C–H bond are responsible for the lines at 1478–1396 cm^{-1}. In the region of 1213–1285 cm^{-1}, stretching vibrations of C–N and C–O bonds are observed. The lines at 1177 and 1132 cm^{-1} are attributed to wagging vibrations of C–H bonds. The lower frequency line at 750 cm^{-1} belongs to the mode characterizing Al–O vibrations and breathing vibrations of the benzene and pyridine rings. The spectra of coordination compounds at wave numbers around 740 cm^{-1} exhibit vibrations of Al–N bonds [17], which are absent in the spectrum of the original HQ. The modes at 625, 548, 540 and 530 cm^{-1} correspond to combined vibrations [ν(Al–O) + ν(Al–N) + δ_{ring}); the modes at 504 and 470 cm^{-1} correspond to vibrations of ring deformations. According to [18], vibrations indicating the formation of Al–O chemical bonds in hydroxyquinolinate molecules appear in the range of 500–520 cm^{-1}. The line at 570 cm^{-1} refers to wagging vibrations of the benzene and pyridine rings and torsional vibrations of Al–O–C. The line at 520 cm^{-1} is attributed to vibrations of Al–O bond stretching and deformation of hydroxyquinoline fragments attached to metal atoms (breathing vibration of benzene and pyridine rings). The frequency of the Al–O stretching vibration mode at 520 cm^{-1} is in satisfactory agreement with the observed value of 523 cm^{-1}, which characterizes the meridional isomer. In turn, this value for the *fac*-isomer is 534 cm^{-1} [19]. Torsional vibrations of Al–O and wagging vibrations of the benzene and pyridine rings are characterized by the line at 504 cm^{-1}. The vibrational mode observed at 750 cm^{-1} can be attributed to the breathing mode of the HQ fragment, while the line at 802 cm^{-1} is attributed to the deformation mode of the HQ ring [20]. The lines at 591, 460 and 445 cm^{-1} characterize the torsional vibrations of the C–H bond. The line at 405 cm^{-1} can be attributed to vibrations of ring deformation and Al–O bond stretching.

The Raman spectrum of HQ (Table 3) has a more pronounced vibrational structure compared to Alq_3 spectrum (Fig. 6, spectrum *2*). Symmetrical vibrations of aromatic rings are characterized by high intensity. Thus, symmetrical vibrations of C–C bonds are active in the regions of 1590 and 1410 cm^{-1}.

The peak at 1480 cm^{-1} characterizes the C–C bond stretching mode. The HQ vibration peak located at 1437 cm^{-1} is characterized by δ(C–O–H) wagging and C–C bond stretching modes. Three intense bands at 1352, 1387 and 1437 cm^{-1} characterize vibrations of ring stretching, C–O bonds, and wagging of O–H bonds. The HQ peak located at 1281 cm^{-1} is characterized by C–H bond wagging and C–N stretching modes. The peak at 1232 cm^{-1} characterizes the stretching vibrations of C–C bonds, and at 1212 cm^{-1} it characterizes the stretching vibrations of C–N and C–O bonds. The vibration lines at 800 and 550 cm^{-1} are attributed to the HQ ring deformation mode [20]. The line at 752 cm^{-1} is attributed to the HQ breathing mode. The band at 723 cm^{-1} corresponds to highly symmetrical vibrations of the quinoline rings [21]. The spectrum contains a band at 644 cm^{-1}, which characterizes vibrations of ring stretching and wagging of C–H bonds. The lines at 585 and 479 cm^{-1} are responsible for the stretching vibrations of C–O bonds. The bands at 272, 180 and 167 cm^{-1} are responsible for the torsional vibrations of the quinoline rings.

3.3. Spectrophotometric study of Alq_3 *solvents*

UV-visible absorption spectroscopy has been used to characterize solvents of Alq_3 in various organic solvents [22–26]. The spectra were obtained under the same conditions. Figure 7 shows the UV/VIS absorption spectra of Alq_3 in the short-wavelength region of the spectrum in the following solvents: EtOH, *i*-PrOH, TEP, toluene.

Solvents of α-Alq_3 absorb significantly in the UV region and have several absorption lines here. Table 4 shows the spectral characteristics of α-Alq_3 ($C = 8.0 \cdot 10^{-6}$ M) in various solvents in the UV region of the spectrum. The lines of electronic transitions are located in the mid-UV region from 226 to 285 nm. The clearest absorption line is observed at 255–258 nm and has ε_{max} from ~59000 to 102000 $L \cdot (mol \cdot cm)^{-1}$.

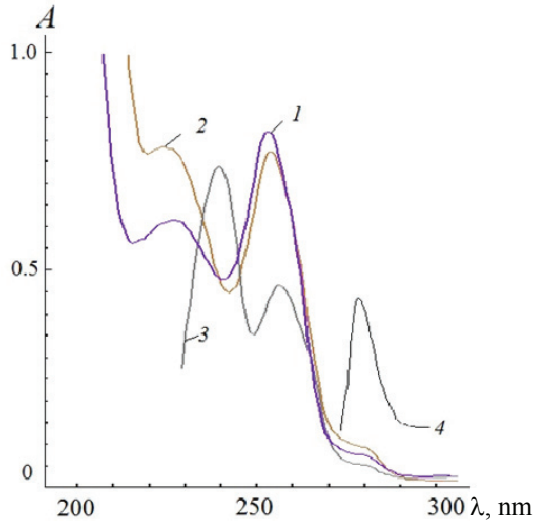

Fig. 7. UV/VIS absorption spectra of Alq_3 ($C = 8.0 \cdot 10^{-6}$ M) in organic solvents: EtOH (*1*), *i*-PrOH (*2*), TEP (*3*), toluene (*4*)

Figure 8 shows the absorption spectra in the range of 300–500 nm of solvents of α-Alq_3 (sample IV) with a concentration of $C = 1.7 \cdot 10^{-4}$ M in eight solvents: DMSO, CH_3CN, EtOH, *i*-PrOH, TEP, $CHCl_3$, 1,4-dioxane , toluene.

Table 5 shows the spectral characteristics of α-Alq_3 in various solvents ($C = 1.7 \cdot 10^{-4}$ M) in the wavelength range of 300–500 nm. The spectra contain two bands with insignificant absorption: λ_{max}^{I} is in the range of 315–320 nm, ε^{I} takes values from 2676 to 4765 $L \cdot (mol \cdot cm)^{-1}$; λ_{max}^{II} is in the range of 330–335 nm and ε^{II} takes values from 2824 to 4412 $L \cdot (mol \cdot cm)^{-1}$ (Table 4).

Table 4. Spectral characteristics of α-Alq_3 ($C = 8.0 \cdot 10^{-6}$ M) in various solvents

λ_{max}, nm / A	EtOH	*i*-PrOH	TEP	Toluene
λ_{max}^{I}, nm / A^{I}	228 / 0.62	226 / 0.78	241 / 0.74	–
ε^{I}, $L \cdot (mol \cdot cm)^{-1}$	77500	97500	92500	
λ_{max}^{II}, nm / A^{II}	255 / 0.82	255 / 0.77	258 / 0.47	
ε^{II}, $L \cdot (mol \cdot cm)^{-1}$	102500	96250	58750	
λ_{max}^{III}, nm / A^{III}	285 / 0.13*	285 / 0.11*	285 / 0.10*	283 / 0.43
ε^{III}, $L \cdot (mol \cdot cm)^{-1}$	16250	13750	12500	53750

* shoulder.

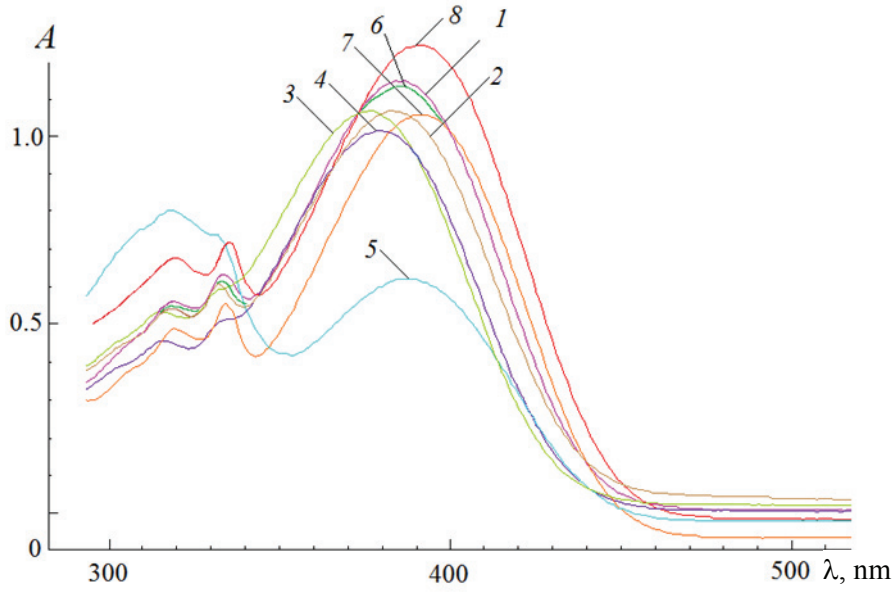

Fig. 8. UV/VIS absorption spectra of Alq_3 in the visible region of the spectrum ($C = 1.7 \cdot 10^{-4}$ M) in organic solvents: DMSO (*1*), CH_3CN (*2*), EtOH (*3*), *i*-PrOH (*4*), TEP (*5*), $CHCl_3$ (*6*), 1,4-dioxane (*7*), toluene (*8*)

Table 5. Spectral characteristics of α-Alq_3 ($C = 1.7 \cdot 10^{-4}$ M) in various solvents

λ_{max}, nm / A	DMCO	CH_3CN	EtOH	*i*-PrOH	TEP**	$CHCl_3$	1,4-dioxane	Toluene
Rel. diel. solvent permeability, ε	46.7	37.5	24.6	17.9	8	4.8	2.3	2.4
Dipole moment μ, *D*	3.9	3.45	1.68	1.66	3.03	1.15	0.45	0.43
λ_{max}^{I}, nm / A^{I} ε^{I}, L·(mol·cm)$^{-1}$	319 / 0.56 3294	317 / 0.54 3159	315 / 0.50 2912	317 / 0.46 2676	318 / 0.81 4765	318 / 0.52 3024	319 / 0.49 2882	320 / 0.68 4000
λ_{max}^{II}, nm / A^{II} ε^{II}, L·(mol·cm)$^{-1}$	333 / 0.63 3706	332 / 0.61 3565	330 / 0.51* 3000	330 / 0.48* 2824	332 / 0.75 4412	334 / 0.55 3206	334 / 0.56 3294	335 / 0.72 4235
λ_{max}^{III}, nm / A^{III} ε^{III}, L·(mol·cm)$^{-1}$	386 / 1.15 6765	383 / 1.07 6265	375 / 0.98 5782	379 / 1.02 5965	388 / 0.62 3647	386 / 1.06 6206	392 / 1.06 6235	391 / 1.24 7294

* – shoulder; ** – triethylphosphate.

These bands correspond to π → π* electronic transitions, which is due to the presence of double bonds in the ligand molecule.

Under the influence of a polar solvent, the absorption maxima caused by π → π* transitions shift to the bathochromic (red) side. However, it is impossible to establish an unambiguous pattern in the systems under consideration. Thus, in the most polar solvent we are considering, in DMSO, $\lambda_{max}^{I} = 319$ nm, and in toluene $\lambda_{max}^{I} = 320$ nm. The situation is similar with the values of λ_{max}^{II}.

The absorption bands that appear at higher wavelengths in the range 375–392 nm correspond to *n* → π* electronic transitions and can be classified as ligand-centered electronic transitions. These lines are characterized by a molar extinction coefficient in the range of 3647–7294 L·(mol·cm)$^{-1}$. In polar solvents, such absorption lines should shift hypsochromically to the blue region of the spectrum. However, for Alq_3 an unambiguous conclusion about the dependence of the shift of absorption lines on the polarity of the solvent cannot be made.

Electronic *n* → π* transitions are a consequence of the presence of heteroatoms with a lone electron pair in the ligand structure. They are realized as a result of electron density transfer from the highest

occupied molecular orbital (HOMO), which is mainly localized on the phenoxyl ring of HQ ligands, to the lowest unoccupied molecular orbital (LUMO) located on the pyridine ring.

As is known, with increasing solvent polarity, characterized by the Kirkwood function $(\varepsilon - 1/2\varepsilon + 1)$, the lines of $\pi \rightarrow \pi^*$ transitions shift bathochromically due to greater stabilization of more polar excited states in comparison with the ground states; polar proton-donor solvents cause a blue shift of $n \rightarrow \pi^*$ transitions due to greater stabilization of the ground state due to the formation of complexes with hydrogen bonds. Apparently, the intermolecular interaction of Alq_3 in solvents of organic solvents (Sol) is of decisive importance. The nature of Alq_3–Sol intermolecular interactions ultimately determines the spectral characteristics of Alq_3 solvents.

Figure 8 shows characteristic α-Alq_3 absorption lines with maxima in the intervals: $\lambda_{max}^{I} = 315–320$, $\lambda_{max}^{II} = 330–335$ and $\lambda_{max}^{III} = 375–392$ nm. The spectra were obtained for sample IV with a concentration of $C = 1.7 \cdot 10^{-4}$ M. The molar extinction coefficients are in the range: for $\lambda_{max}^{I} = 2676–4765$, for $\lambda_{max}^{II} = 2824–4412$ and for $\lambda_{max}^{III} = 3647–7294$. For comparison, according to [27], a solvent of Alq_3 in CH_2Cl_2 at $\lambda_{max} = 388$ nm is characterized by the value $\varepsilon^{388} = 7000$ L·(mol·cm)$^{-1}$.

In this case, it should also be noted that with a decrease in the polarity of the solvents (from DMSO to toluene), no clearly defined bathochromic shift is observed in the absorption spectra. As a result of the solvatochromic effect, a change in the position and intensity of the absorption lines characteristic of Alq_3 quinoline ligands can be observed. Table 5 shows the wavelengths and intensities of the corresponding absorption lines.

3.4. Quantitative determination of Alq_3 *in i-*PrOH *solvent*

To carry out quantitative analyzes of Alq_3 solvents by the spectrophotometric method and standardize its solvents in organic solvents, a series of dilutions of a standard Alq_3 sample in *i*-PrOH was prepared in the concentration range $(1.6–15.0) \cdot 10^{-5}$ M, at which the Bouguer-Lambert-Beer law is observed. Figure 9 demonstrates the spectra of a series of dilutions of Alq_3solvents in *i*-PrOH. Table 6 shows the data for constructing the calibration line $A = f\,C(\alpha\text{-}Alq_3)$ in *i*-PrOH at the analytical wavelength $\lambda_{max} = 379$ nm.

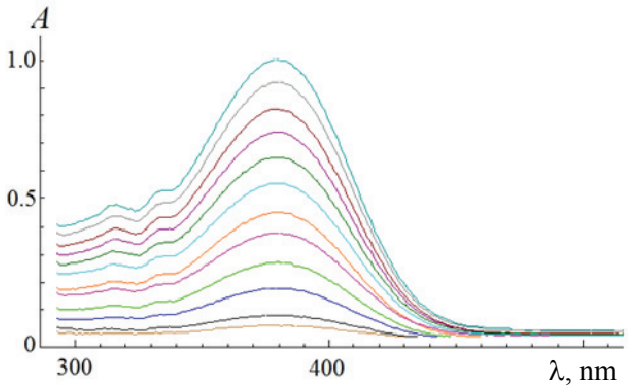

Fig. 9. UV/VIS absorption spectra of α-Alq_3 in *i*-PrOH for constructing a calibration line at $\lambda_{max} = 379$ nm

Table 6. Data for constructing the calibration line $A = fC(\alpha\text{-}Alq_3)$ in *i*-PrOH at $\lambda_{max} = 379$ nm. Calibration chart is on insert

A	$C \cdot 10^5$, M
0.08	1.57
0.18	3.10
0.27	4.58
0.38	6.02
0.45	7.41
0.56	8.76
0.65	10.07
0.74	11.35
0.82	12.59
0.92	13.79
1.00	14.97

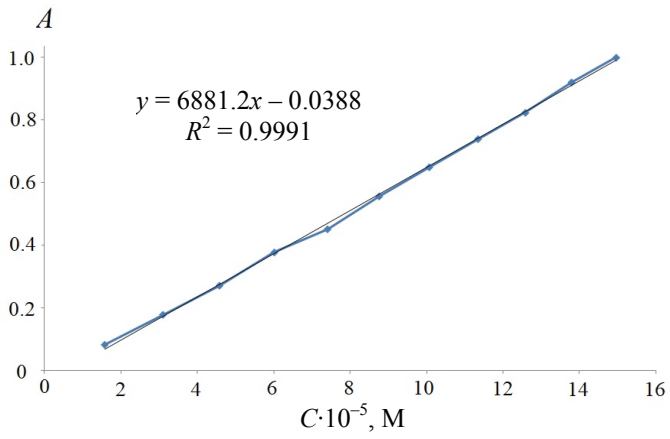

The findings show the possibility of standardizing solvents of α-Alq_3 in organic solvents and its quantification in solvents.

4. Conclusion

This work proposes a simple and original synthesis of the *mer*-isomer of the α-polymorphic modification of tris(8-hydroxyquinolinate) aluminum. The phase composition of the α-phase *mer*-Alq_3 powder obtained by the new method was determined by X-ray diffraction analysis and is in good agreement with the results of Raman spectroscopy. The spectroscopic characteristics of Alq_3 in various solvents were studied. The spectrum of Alq_3 in triethyl phosphate (TEP) is of greatest interest. The spectrum is characterized by the presence of a strong absorption line at 318 nm, the intensity of which is higher than the absorption line at 388 nm. In all other solvents used in the work, the opposite picture was observed. One of the reasons for this behavior may be the formation of Alq_3–TEP complexes (solvates). The specific behavior of the Alq_3 molecule in the solvent is determined by the specific and universal solvation centers present in its structure. In accordance with the types of intermolecular interactions, it is customary to distinguish nonspecific solvation, caused by van der Waals interactions, and specific solvation, which manifests itself as a result of electrostatic interactions, coordination and hydrogen bonds. The stability of specific solvates in the Alq_3–TEP system and, as a consequence, the shape of the absorption spectrum, can be influenced by the viscosity of the solvent. In addition, in viscous solvents, the mutual transformations of different solvates are difficult. All new facts and observations obtained in this work require detailed study and explanation, which will serve as a topic for further research.

5. Funding

This study received no external funding.

6. Acknowledgements

Thanks to G.A. Gevorgyan for conducting research using a scanning electron microscope; S.S. Arsentiev, I.V. Kuzmin for participation in the processing of experimental data.

7. Conflict of interests

The authors declare no conflict of interest.

References

1. Tang CW, VanSlyke SA. Organic electroluminescent diodes. *Applied Physics Letters*. 1987;51(12):913-915. DOI:10.1063/1.98799

2. Costa JCS, Lima CFRAC, Santos LMNBF. Electron transport materials for organic light-emitting diodes: understanding the crystal and molecular stability of the tris(8-hydroxyquinolines) of Al, Ga, and In. *The Journal of Physical Chemistry C*. 2014;118(38): 21762-21769. DOI:10.1021/jp503935k

3. Hongze G, Zhang H, Zhang H, Gen Y, Su ZM. Theoretical study of isomerism/phase dependent charge transport properties in tris(8-hydroxyquinolinato) aluminum(III). *The Journal of Physical Chemistry A*. 2011;115(33):9259-9264. DOI:10.1021/jp202976m

4. Rajeswaran M, Blanton TN, Tang CW. et al. Structural, thermal, and spectral characterization of the different crystalline forms of Alq_3, tris(quinolin-8-olato) aluminum(III), an electroluminescent material in OLED technology. *Polyhedron*. 2009;28(4):835-843. DOI:10.1016/J.POLY.2008.12.022

5. Cherednichenko AG, Avetisov RI, Akkuzina AA, Avetisov IH. Study of the processes of synthesis and purification of aluminum, gallium and indium tri-(8-hydroxyquinolates) for the technology of organic light-emitting devices. *Vestnik Kazanskogo tekhnologicheskogo universiteta*. 2015;18(10):52-54. (In Russ.)

6. Avetisov RI, Akkuzina AA, Cherednichenko AG, Khomyakov AV, Avetissov IC. Polymorphism of tris(8-hydroxyquinoline) aluminum, gallium, and indium. *Doklady akademii nauk = Doklady Chemistry*. 2014;454(1):6-8. DOI:10.1134/S0012500814010029

7. Avetisov R, Kazmina K, Barkanov A. et al. One-step synthesis of high pure tris(8-hydroxyquinoline) aluminum for optics and photonics. *Materials (Basel)*. 2022;15(3):734-741. DOI:10.3390/ma15030734

8. Kazmina KV, Pytchenko AA, Li YaR, Tonova LD, Zakharova AV, Myagkova EV, Tashlintseva SA, Zykova MP, Avetisov RI. Synthesis and luminescent properties of aluminum tri-(8-hydroxyquinolate). *Uspekhi v khimii i khimicheskoy tekhnologii*. 2021;35(6):43-46. (In Russ.)

9. Katakura R, Koide Y. Configuration-specific synthesis of the facial and meridional isomers of tris(8-hydroxyquinolinate)aluminum (Alq_3). *Inorganic Chemistry*. 2006;45(15):5730-5732. DOI:10.1021/ic060594s

10. Rulfs CL. A text-book of quantitative inorganic analysis including elementary instrumental analysis. *Inorganic Chemistry*. 1962;1(3):723-724. DOI:10.1021/ ic50003a063

11. Painuly D, Mogha NK, Masram DT. et al. Phase stability and transformation of the α to ε-phase of Alq_3 phosphor after thermal treatment and their photo-physical properties. *Journal of Physics and Chemistry of Solids*. 2018;121:396-408.. DOI:10.1016/j.jpcs.2018.05.035

12. Brinkmann M, Gadret G, Muccini M. et al. Correlation between molecular packing and optical properties in different crystalline polymorphs and amorphous thin films of mer-tris(8-hydroxyquinoline)

aluminum(III). *Journal of the American Chemical Society*. 2000;122:5147-5157. DOI:10.1021/JA993608K

13. Rajeswaran M, Blanton TN, Tang CW. et al. Structural, thermal, and spectral characterization of the different crystalline forms of Alq_3, tris(quinolin-8-olato) aluminum(III), an electroluminescent material in OLED technology. *Polyhedron*. 2009;28(4):835-843. DOI:10.1016/j.poly.2008.12.022

14. Fukushima T, Kaji H. Green- and blue-emitting tris(8-hydroxyquinoline)aluminum(III) (Alq_3) crystalline polymorphs: Preparation and application to organic light-emitting diodes. *Organic Electronics*. 2012;13(12):2985-2990. DOI:10.1016/j.orgel.2012.08.036

15. Rajeswaran M, Blanton TN. Single-crystal structure determination of a new polymorph (ε-Alq_3) of the electroluminescence OLED (organic light-emitting diode) material, tris(8-hydroxyquinoline)aluminum (Alq_3). *Journal of Chemical Crystallography*. 2005;35(1):71-76. DOI:10.1007/s10870-005-1157-4

16. Halls MD, Aroca R. Vibrational spectra and structure of tris(8-hydroxyquinoline)aluminum(III). *Canadian Journal of Chemistry*. 1998;76:1730-1736. DOI:10.1139/v98-182

17. Patel KD, Patel HS. Synthesis, spectroscopic characterization and thermal studies of some divalent transition metal complexes of 8-hydroxyquinoline. *Arabian Journal of Chemistry*. 2013;10:S1328-S1335. DOI:10.1016/j.arabjc.2013.03.019

18. Hui L, Yuqin F, Linbo Z. et al. In situ route to novel fluorescent mesoporous silica nanoparticles with 8-hydroxyquinolinate zinc complexes and their biomedical applications. *Microporous and Mesoporous Materials*. 2012;151:293-302. DOI:10.1016/j.micromeso.2011.10.021

19. Peng J, Zhang S-J, Wang K, Dove M. Density functional theory calculation of spectrum and excitation properties of mer-Alq_3. *Acta Physica Sinica*. 2020;69(2): 023101. DOI:10.7498/aps.69.20191453

20. Dasi G, Lavanya T, Suneetha S, Vijayakumar S, Shim J-J, Thangaraju K. Raman and X-ray photoelectron spectroscopic investigation of solution processed Alq_3/ZnO hybrid thin films. *Spectrochimica Acta Part A: Molecular and Biomolecular Spectroscopy*. 2022;265:120377. DOI:10.1016/j.saa.2021.120377

21. Sowa M, Wala M, Blacha-Grzechnik A. et al. Corrosion inhibitor-modified plasma electrolytic oxidation coatings on 6061 aluminum alloy. *Materials*. 2021;14(3):619. DOI:10.3390/ma14030619

22. Alzahrani H, Sulaiman K, Mahmoud AY, Bahabry RR. Study of organic visible-blind photodetector based on Alq3:NPD blend for application in near-ultraviolet detection. *Optical Materials*. 2020;110:110490. DOI:10.1016/j.optmat.2020.110490

23. Alzahrani H, Sulaiman K, Muhammadsharif FF. et al. Effect of illumination intensity on a self-powered UV photodiode based on solution-processed NPD: Alq_3 composite system. *Journal of Materials Science: Materials in Electronics*. 2021;32:14801-14812. DOI:10.1007/s10854-021-06034-x

24. Omar WAE. Synthesis and photophysical properties of aluminium tris-(4-morpholine-8-hydroxyquinoline). *Journal of Advanced Research*. 2013;4(6):525-529. DOI:10.1016/j.jare.2012.09.003

25. Hoshi T, Kumagai K, Inoue K. et al. Electronic absorption and emission spectra of Alq_3 in solution with special attention to a delayed fluorescence. *Journal of Luminescence*. 2008;128(8):1353-1358. DOI:10.1016/j.jlumin.2008.01.003

26. Heiskanen JP, Tolkki AE, Lemmetyinen HJ, Hormi OEO. Fused Alq_3 derivatives: syntheses and photophysical characteristics. *Journal of Materials Chemistry*. 2011;21(38):14766-14775. DOI:10.1039/c1jm12424b

27. Montes VA, Pohl R, Shinar J, Anzenbacher P. Effective manipulation of the electronic effects and its influence on the emission of 5-substituted tris(8-quinolinolate)aluminum(III) complexes. *Chemistry: A European Journal*. 2006;12(17):4523-4535. DOI:10.1002/chem.200501403

Information about the authors / Информация об авторах

Denis V. Belov, Cand. Sc. (Chem.), Associate Professor, Senior Researcher, Federal Research Center A.V. Gaponov-Grekhov Institute of Applied Physics of the Russian Academy of Sciences (IAP RAS), Nizhny Novgorod, Russian Federation; Leading Technologist, Institute of Physics of Microstructures of the Russian Academy of Sciences (IPM RAS), Nizhny Novgorod, Russian Federation; ORCID 0000-0001-7190-0477; e-mail: belov.denbel2013@yandex.ru

Sergey N. Belyaev, Cand. Sc. (Chem.), Researcher, Head of Laboratory, IAP RAS, Nizhny Novgorod, Russian Federation; Leading Technologist, IPM RAS, Nizhny Novgorod, Russian Federation; ORCID 0000-0003-2346-9103; e-mail: serg_belyaev@bk.ru

Белов Денис Владимирович, кандидат химических наук, доцент, старший научный сотрудник, Институт прикладной физики им. А. В. Гапонова-Грехова РАН (ИПФ РАН), Нижний Новгород, Российская Федерация; ведущий технолог, Институт физики микроструктур РАН (ИФМ РАН), Нижний Новгород, Российская Федерация; ORCID 0000-0001-7190-0477; e-mail: belov.denbel2013@yandex.ru

Беляев Сергей Николаевич, кандидат химических наук, научный сотрудник, заведующий лабораторией, ИПФ РАН, Нижний Новгород, Российская Федерация; ведущий технолог, ИФМ РАН, Нижний Новгород, Российская Федерация; ORCID 0000-0003-2346-9103; e-mail: serg_belyaev@bk.ru

Pavel A. Yunin, Cand. Sc. (Phys. and Math.), Sciences Researcher, Head of Laboratory, IPM RAS, Nizhny Novgorod, Russian Federation; ORCID 0000-0001-7081-2934; e-mail: yunin@ipmras.ru

Dmitry B. Radishev, Cand. Sc. (Phys. and Math.), Senior Researcher, IAP RAS, Nizhny Novgorod, Russian Federation; ORCID 0000-0002-8416-1738; e-mail: dibr@ipfran.ru

Юнин Павел Андреевич, кандидат физико-математических наук, научный сотрудник, заведующий лабораторией, ИФМ РАН, Нижний Новгород, Российская Федерация; ORCID 0000-0001-7081-2934; e-mail: yunin@ipmras.ru

Радищев Дмитрий Борисович, кандидат физико-математических наук, старший научный сотрудник, ИПФ РАН, Нижний Новгород, Российская Федерация; ORCID 0000-0002-8416-1738; e-mail: dibr@ipfran.ru

Received 26 July 2023; Accepted 10 October 2023; Published 15 December 2023